

Role of Electronic, Geometric, and Surface Properties on the Mechanism of the Electrochemical Hydriding/Dehydriding Reactions

S. Srinivasan^a, W. Zhang^a, M.P.S. Kumar^a, A. Visintin^a, S. Mukerjee^b, J. McBreen^b, G. Adzic^b,
J.R. Johnson^b, J.J. Reilly^b, R.B. Schwarz^c, M.L. Wasz^c and H.S. Lim^d

^a Center for Electrochemical Systems and Hydrogen Research, Texas Engineering Experiment Station,
Texas A&M University System, College Station, TX 77843-3402

^b Department of Applied Science, Brookhaven National Laboratory, Upton, New York 11973

^c Center for Materials Science, Los Alamos National Laboratory, Los Alamos, NM 87545

^d Hughes Aircraft Company, Electro Dynamics Division, Torrance, CA 90505

RECEIVED
MAR 05 1996
OSTI

ABSTRACT

Since 1990 there has been an ongoing collaboration among the authors to investigate the role of individual elements on the thermodynamics and kinetics of hydriding/dehydriding reactions. This review article presents the electrochemical and physicochemical characteristics of hydriding/dehydriding reactions from the point of view of their dependence on electronic, geometric and surface properties of the hydride materials. X-ray absorption spectroscopy (XAS), x-ray diffraction spectroscopy (XRD) and scanning vibrating electrode technique (SVET) studies were carried on AB₃ type alloys, partially substituted by other elements. Expansion of the unit cell volume and a larger Ni d band vacancy are beneficial for increasing the amount of the hydrogen storage. XAS and SVET showed that the Ce substitution for La in an AB₃ alloy enhances the lifetime of hydride electrode.

Alloys for Hydride Electrodes in Nickel/Metal Hydride Batteries

Effect of Method of Preparation of Alloys on Performance of Hydride Electrodes. — The AB₃ type alloys were prepared by (i) arc-melting of the constituent elements, 99.99% purity, in a MRC model AF-92C arc furnace which provides a low pressure, inert gas atmosphere to minimize contamination, followed by annealing in an argon atmosphere at 800° C for three days. Elements of the desired composition were melted two to four times and held in the liquid state for 20 - 30 seconds to ensure complete mixing and formation of a homogeneous alloy; (ii) mechanical alloying (ball-milling) for four hours using a SPEX 8000 mixer/mill, which was carried out in a tungsten carbon vial in an argon glovebox containing less than 1 ppm oxygen, followed by annealing in an open fused silica tube at 800° C for 30 minutes.

The electrochemical characterization studies consisted of measurements of: (i) initial capacity; and (ii) rate capability. All electrodes were prepared with teflonized carbon (Vulcan XC-72). An alloy, prepared by mechanical alloying/annealing, has a slightly lower electrochemical hydriding capacity, compared with an alloy of with the same composition prepared by arc-melting/annealing, as illustrated in Fig. 1. The P-C-T

isotherm of the samples confirms the same behavior for gas phase hydriding. The probable reason for this result is the incomplete alloying of samples prepared by mechanical alloying. However, the rate capability of the hydride electrode prepared using the sample prepared by mechanical alloying/annealing was higher than that of the sample prepared by conventional arc-melting, Fig. 2.

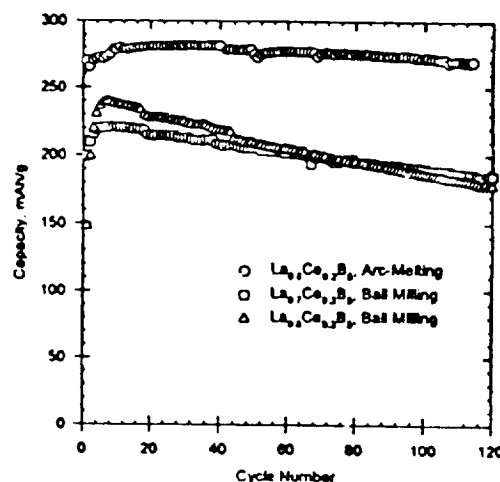


Fig. 1. Cycle life studies on AB₃ alloys prepared by ball milling (BM) and arc-melting (AM).

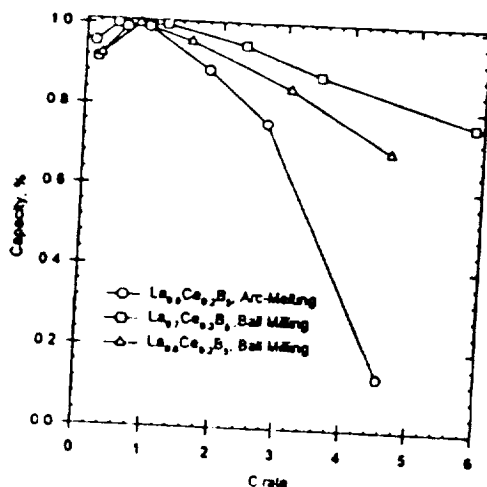


Fig. 2. Comparison of rate capabilities of substituted AB_3 alloys prepared by ball milling (BM) and arc-melting (AM).

Correlations Between Gas Phase and Electrochemical Hydriding/Dehydriding Characteristics. — The gas phase hydrogen absorption/desorption characteristics of metallic hydrides are typically described by the pressure-composition-temperature (P-C-T) isotherms (1); a schematic representation of this isotherm is shown in Fig. 3.

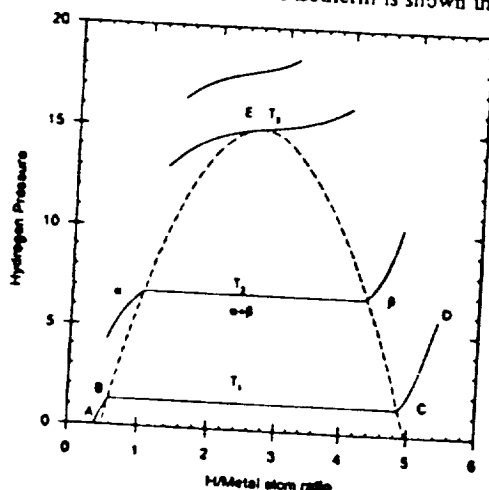


Fig. 3. Schematic representation of the P-C-T isotherms for hydrogen-metal system.

Extent of hydrogen absorption depends on the equilibrium pressure. At relatively low pressures, the absorbed hydrogen atoms begin to occupy the interstitial sites in the metal lattice and the isotherm ascends steeply as hydrogen dissolves in the metal, forming a solid solution, designated as the α phase. Region A-B signifies the limited solution of hydrogen in the metal alloy. The region B-C represents the

appearance of a second phase which is in equilibrium with the saturated solid-solution (i.e., the α phase). The second phase is usually referred to as the β phase. This is the phase which contains the large amount of hydrogen absorbed in the alloy. Thus, according to Gibbs' phase rule, the pressure must be constant — the plateau pressure, in the two phase region (α and β). After all the hydride material is converted into the β phase (region C-D), further absorption of hydrogen is very difficult. Thus, the equilibrium pressure increases sharply with amount of absorbed hydrogen.

The equilibrium potential of the hydride electrode in 6M KOH solution at $T=298^\circ\text{K}$ can be obtained from the free energy change of the hydriding reaction and is given by the following equation:

$$E_m = -\frac{RT}{2F} \ln P_{H_2} = -0.0291 \log_{10} P_{H_2} \quad (1)$$

where P_{H_2} is the equilibrium hydrogen pressure, F is the Faraday constant and E_m is the potential vs. the reversible hydrogen electrode (RHE). Equation (1) correlates the equilibrium pressure of the hydriding/dehydriding reaction in the gas phase with the electrochemical equilibrium potential of the redox couple. Furthermore, since equation (1) applies to the equilibrium plateau pressure region (B-C section in Fig. 3), the potential of the metal hydride electrode is approximately constant during the charge and discharge processes; the potential changes only by about 29 mV for an order of magnitude change of the equilibrium hydrogen pressure.

The equilibrium pressure of hydrogen is one of the important factors which influences the behavior of the metal hydride batteries. Capacity retention is defined as the percentage of the capacity remaining after the storage period with respect to the initial capacity. For a hydride alloy with the lower plateau pressure, the capacity retention is usually higher and vice versa. This is because lower the equilibrium pressure, the higher is the stability of the hydride state; the capacity retention of the hydride electrodes with alloys having different plateau pressures, is shown in Fig. 4.

On the other hand, the plateau pressure of the hydride material cannot be very high (3), because the charge efficiency of metal hydride battery will be lower, leading to hydrogen evolution and a lower capacity of the battery. Hydrogen absorption pressure-composition isotherms for some intermetallic compounds are presented in Fig. 5. Sn and Co substitution are effective for lowering the hydrogen plateau pressure, whereas the reverse effect is observed with Ce substitution. Sn substitution lowers the plateau pressure with a slight decrease of the overall hydrogen storage capacity. Ce and Co substitution, in addition to affecting the plateau pressure, decreases hydrogen storage capacity. BNL23 which contains only Ce

and Co substituents and no Sn has a relative higher plateau pressure. The electrochemical performance characteristics of these hydride electrodes (electrochemical capacity

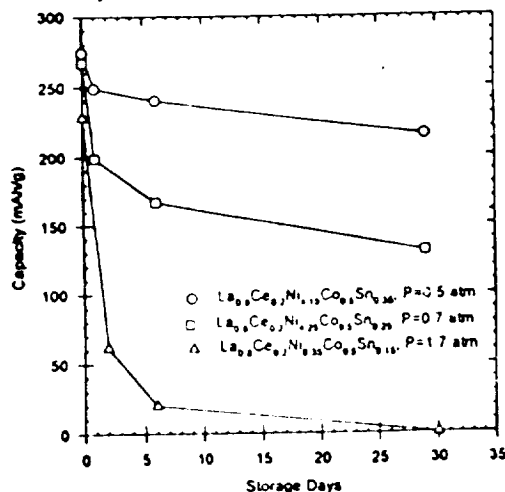


Fig. 4. Capacity retention of hydride electrodes dependent on the plateau pressure.

and cycle-life behavior) are presented in Fig. 6. BNL23 has the maximum amount of hydrogen absorption per formula unit. However, since the plateau pressure is quite high (> 3 atm), the BNL 23 has a very low discharge capacity. For the practical metal-hydride battery, the plateau pressure

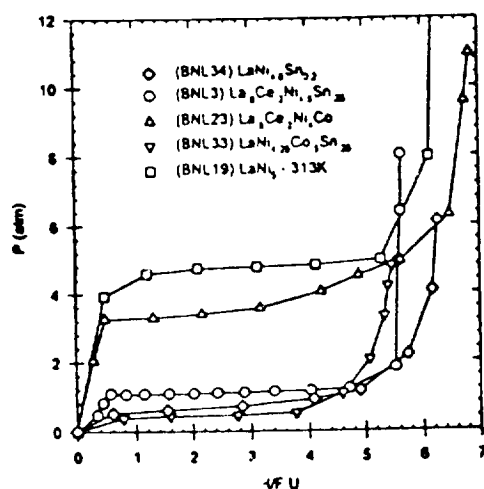


Fig. 5. Hydrogen absorption pressure-composition isotherms for substituted AB_3 intermetallics at 298K.

is usually below 1 atm, which could be attained by partial substitution of elements in the AB_3 alloys. By substituting with Sn, the plateau is decreased and the electrochemical capacity increased. However, a careful optimization of the amounts of the individual substituents is necessary to retain high hydriding capacities and good cycle life.

Effect of Electronic Properties on Electrochemical Hydriding/Dehydriding Characteristics

X-Ray Absorption Studies. — X-ray absorption spectroscopy (XAS) has the ability to probe *in-situ*, both electronic (from X-ray absorption near edge structure, XANES) and geometric parameters (from the extended X-ray absorption fine structure, EXAFS) of the alloys. Figure 7 shows normalized Ni K edge XANES spectra for the three dry uncycled electrodes. The edge is shifted by about 1.5 eV below that found for a Ni foil. Substitutions by Ce and Sn decrease the peak at 0.0 eV. Absorption at the K edge is due to the excitation of $1s$ electrons. Because of the selection rules only transitions into empty $4p$ states

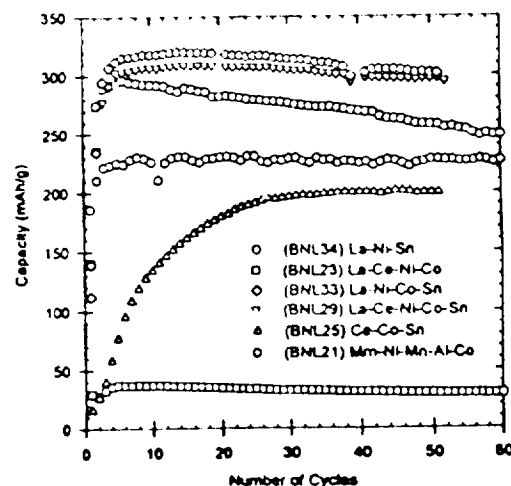


Fig. 6. Cycle-life behavior of hydride electrodes containing substituted AB_3 intermetallics, at C/2 charge and discharge rates. Temperature 298K.

are allowed. In systems with cubic or octahedral symmetry, weak quadrupole transitions are observed as small pre-edge peaks in the XANES spectra (4). Due to the hexagonal symmetry of the alloys, there is mixing of p and d states and, as a result, transitions into the empty p part of these mixed $p-d$ states occur. Theoretical calculations of the density of states (DOS) by Gupta (5) have shown that the Fermi level of $LaNi_3$ falls rapidly, decreasing the extent of Ni d bands which are not fully filled. Thus the intensity of the peak at 0.0 eV can be taken as an indirect measure of the number of empty Ni d states. The reduction in the intensity of this peak on the addition of Sn and Ce is due to either a partial filling of the Ni d states, a reduction in symmetry by lattice distortion, or both.

Although Sn substitution increases the unit cell volume, which accounts for the lower plateau pressure (see next section), the decrease in hydrogen storage capacity

is due to the electronic effects, which is similar to the loss in hydrogen capacity in $\text{LaNi}_{1-x}\text{Al}_x$ proposed by Gscheidner, *et al.* (6), in which the partial filling of the alloy's 3-d band is due to electron donation by Al. This filling decreases the number of holes that can be occupied by the electrons from the hydrogen.

Effect of Geometric Properties on Electrochemical Hydriding/Dehydriding Characteristics

X-Ray Diffraction Studies. — Table I shows the results of X-ray diffraction analysis for the alloys. All the alloys are single phase and have the hexagonal CaCu_5 type structure, typical of the AB_5 type alloys. As indicated by the lattice parameters in Table I, substitution of B component (Ni) by Sn in the AB_5 metal hydride lattice (LaNi_5) results in an increase in the lattice parameters and hence the cell volume. However, substitution of the A component (La) with Ce causes a minor shrinkage along the a axis. The structural change, due to partial substitution of Ni by Sn, is reflected in the lowering of the hydrogen plateau pressure which could thus improve the charging efficiency and the capacity retention of the hydride electrode. This structure change

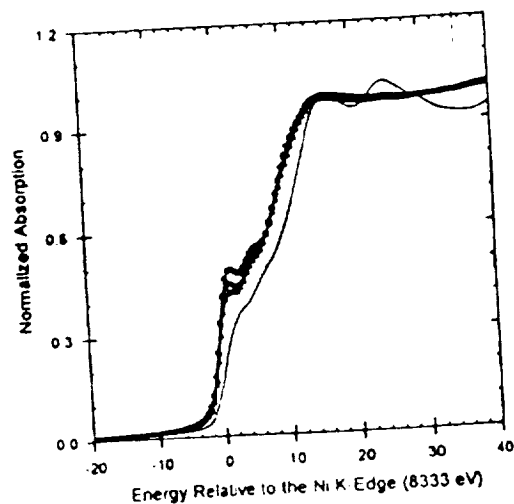


Fig. 7. Comparison of the Ni K edge XANES for LaNi_5 (O), $\text{LaNi}_{4.8}\text{Sn}_{0.2}$ (●), and $\text{La}_{0.8}\text{Ce}_{0.2}\text{Ni}_{4.8}\text{Sn}_{0.2}$ (Δ) in dry uncharged electrodes relative to the pure Ni foil (—) data.

Table I. Physico-chemical Properties of Modified AB_5 Type Alloys

Composition	Lattice Parameters $a, \text{\AA}$ $c, \text{\AA}$		Cell Volume (\AA^3)	Plateau Pressure ^(a) atm.	H_{max}/FU	$V_H (\text{\AA})^3$	Initial Capacity (mAh/g)
LaNi_5	5.009	3.970	86.31	1.80	6.90	3.5	350
$\text{LaNi}_{4.8}\text{Sn}_{0.2}$	5.0557	4.019	88.96	1.01	6.26	3.2	296
$\text{La}_{0.8}\text{Ce}_{0.2}\text{Ni}_{4.8}\text{Sn}_{0.2}$	5.033	4.038	88.6	1.08	5.73	-	315

(a) All reported values are at a temperature of 299°K

due to substitution is also reflected in the reduced molar volume of hydrogen (V_H). The electrochemical capacity of the metal hydride electrodes are also given in Table I.

Effect of Surface Properties on Electrochemical Hydriding/Dehydriding Characteristics

While certain AB_5 alloys are attractive for replacements of cadmium electrodes in nickel-cadmium batteries, the parent alloy, LaNi_5 , is not suitable because its performance decays rapidly in the battery environment. Corrosion has been, in general, attributed to the degradation mechanism of a hydride electrode. Iwakura *et al.* (7) demonstrated the formation of the corrosion product, $\text{La}(\text{OH})_3$, during a two-day storage period of a LaNi_5Cu anode by comparing the x-ray diffraction patterns recorded before and after the storage. It is necessary to

experimentally detect the formation of corrosion products after electrochemical charge/discharge cycles and also to determine the effect of substitution on the corrosion behavior of modified AB_5 alloys ($\text{B}=\text{Ni}_{1.55}\text{Co}_{0.75}\text{Mn}_{0.4}\text{Al}_{0.3}$). This section reports on (i) the formation corrosion products after 100 electrochemical charge/discharge cycles, as detected by XAS; (ii) a detailed investigation of the local corrosion processes by examining the surfaces of several AB_5 metal hydride electrodes using the scanning vibrating electrode technique (SVET) (8).

X-Ray Absorption Studies (XANES results). — Fig. 8 shows the normalized Ni K edge XANES spectra for LaB_5 before and after electrochemical cycling (100 times) and for a dry $\beta\text{-Ni}(\text{OH})_2$ electrode. Appearance of a white line for the cycled LaB_5 electrode clearly indicates corrosion of the Ni surface and formation of the corrosion product, $\text{Ni}(\text{OH})_2$. Comparison of the area under this peak with that for the β -

Ni(OH)_2 was used to estimate the degree of corrosion. It indicates that 18% of the Ni has corroded. Fig. 9 compares the white lines for LaB_3 , $\text{La}_{0.8}\text{Ce}_{0.2}\text{B}_3$ and MmB_3 after 100 cycles with that for a dry $\beta\text{-Ni(OH)}_2$ electrode. As evident from this figure, the addition of Ce, significantly lowers the Ni corrosion to 8% after 100 cycles. The lack of the white line, in the case of MmB_3 alloy, indicates that there was almost no corrosion of the MmB_3 prepared from the commercially available Mm electrodes.

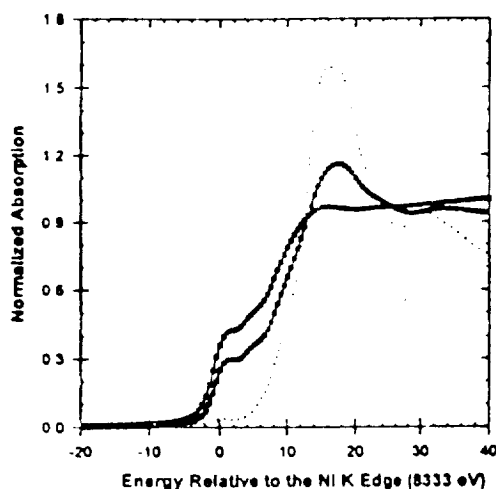


Fig. 8. Ni K edge XANES for LaB_3 electrode before and after cycling. Ni(OH)_2 (....), Uncycled LaB_3 (\square), LaB_3 after 100 cycles (\blacksquare).

Scanning Vibrating Electrode Techniques Studies. — SVET, under open circuit condition, measures the anodic and cathodic current flow on a polished electrode surface in contact with an electrolyte. From the surface studies, it is possible to elucidate the mechanism of chemical and electrochemical oxidation of the alloy causing the deterioration of hydriding alloys and the effect of rare earth substitution in the A component of an AB_3 type alloy on the degradation rate of a hydride electrode and on its corrosion rate. For this purpose, one-dimensional vibrating probe, which consists of an insulated platinum wire with only its tip exposed to the solution, is caused to vibrate perpendicular to the flat electrode surface at a certain frequency (200 Hz). The probe measures the potential gradient in the solution at a certain height over and very close to the electrode surface. This potential gradient results from the current flow due to localized anodic and cathodic sites for electrochemical corrosion. The measured electric field, which is converted to the current density using Ohm's law, normal to the surface, gives the current density distribution map across the surface.

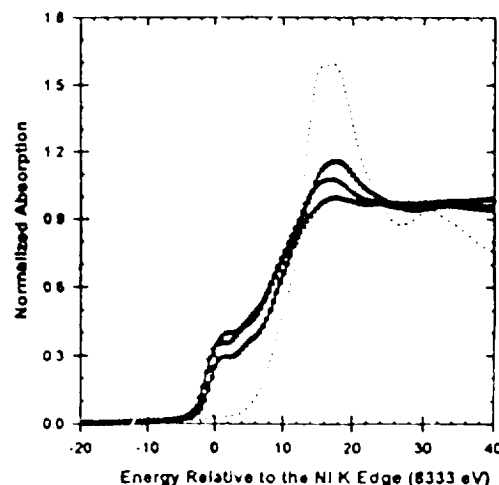


Fig. 9. Ni K edge XANES for electrodes after 100 cycles. LaB_3 (\blacksquare), $\text{La}_{0.8}\text{Ce}_{0.2}\text{B}_3$ (\bullet), MmB_3 (\blacktriangle) and Ni(OH)_2 (....).

The SVET scans on a prototype unsubstituted sample, LaB_3 , (Fig. 10), serves as a reference. The observed current densities are large with several localized anodic regions (positive current) and cathodic regions (negative current). The steady state current density distribution was usually reached after 6 hours immersion. For the samples with La partially substituted by 20% of Ce, i.e., $\text{La}_{0.8}\text{Ce}_{0.2}\text{B}_3$, the normal anodic current density decreased to less than $20 \mu\text{A}/\text{cm}^2$, comparing with $80 \mu\text{A}/\text{cm}^2$ for the LaB_3 alloy. In addition, the number of

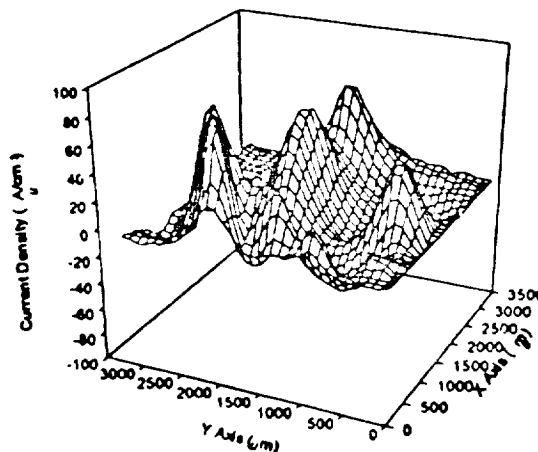


Fig. 10. Three-D plot of the normal current density distribution for LaB_3 flat electrode immersed in 0.01 M KOH solution.

corrosion sites significantly decreased (Fig. 11). With increasing amount of Ce, as for the sample of $\text{La}_{0.95}\text{Ce}_{0.05}\text{B}_5$, even smaller anodic and cathodic currents were recorded. These facts are consistent with the view that Ce inhibits electrode corrosion. All these results strongly suggest that decreased corrosion current for the Ce containing alloys is due to the formation of a passivating film, probably CeO_2 on the electrode surface; this finding is consistent with the previous XAS studies

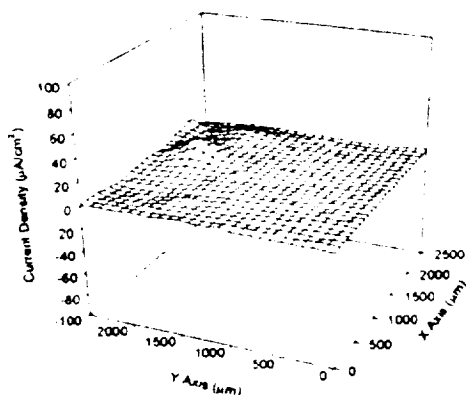


Fig. 11. Three-D plot of the normal current density distribution for $\text{La}_{0.95}\text{Ce}_{0.05}\text{B}_5$ flat electrode immersed in 0.01 M KOH solution.

Conclusion

The following conclusions can be derived from this review paper:

- Alloys prepared by arc-melting/annealing, have higher specific capacities than alloys prepared by mechanical alloying/annealing. The opposite behavior was observed for rate capabilities.
- Substituents leading to an expansion of the unit cell, are beneficial in lowering the hydrogen absorption/desorption plateau pressures to values below 1 atm, which is essential to achieve high electrochemical capacities.
- The XANES results at the Ni K edge indicates that the alloying process results in hybridization of the 4p and 3d orbitals of Ni. The addition of Sn and Ce decreases the number of Ni d band vacancies. This could account for both the decreased hydrogen content and the reduced plateau pressures.
- The XRD analysis results show that the effect of substitution of Ni and Sn causes an increase in the lattice parameters primarily along the c-axis. This manifests itself in a corresponding increase in the unit cell volume. Substitution of La by Ce, however, causes a minor contraction in the cell volume.

- Correlation of the electrochemical and XAS results show that capacity loss is directly related to the extent of Ni corrosion.
- The reduced corrosion current in the Ce containing electrode, as measured using SVET technique, is consistent with XAS results, which showed that the presence of Ce in a homogenous series of AB_5 alloys has a beneficial effect on electrode lifetime.

Acknowledgments

The authors wish to acknowledge the sponsorship of this work by the Chemical Sciences Division, Office of Basic Energy Sciences, U.S. Department of Energy (Contract No. DE-FG03-93ER14381), Hughes Aircraft Company (Contract No. 3-939320-US60) and the NASA Center for Space Power at the Texas A&M University (Grant No. NAGW-1194). The authors gratefully acknowledge the support of the U.S. Department of Energy, Brookhaven National Laboratory (Contract # DEA-CO2-76CH00016) for its role in the development and operation of the National Synchrotron Light Source (NSLS). The experimental work at Brookhaven was supported by the Chemical Sciences Division, Office of Basic Energy Sciences, U.S. Department of Energy (Contract No. DEA-CO2-76CH00016).

References

- F. A. Kuipers, *Phillips Res. Repts. Suppl.*, **2**, 4, (1973).
- J. Balej, *Int. J. Hydrogen Energy*, **10**, 365 (1985).
- C. Iwakura, T. Asaoka, H. Yoneyama, T. Sakai, H. Ishikawa and K. Ogura, *Nippon Kagaku Kaishi*, 1482 (1988).
- A. N. Mansour, C. A. Melendres, M. Pankuch and R. A. Brizzolara, *J. Electrochem. Soc.*, **141**, L69 (1994).
- M. Gupta, *J. Less Common Metals*, **130**, 219 (1987).
- K. A. Gschneider, Jr., T. Takeshita, Y. Chung, and O. D. McMaster, *J. Phys. F: Met. Phys.*, **12**, L1 (1982).
- C. Iwakura, Y. Kajiya, H. Yoneyama, T. Sakai, K. Ogura, and H. Ishikawa, *J. Electrochem. Soc.*, **136**, 1351 (1989).
- H. S. Isaacs and A. J. Davenport, *AIChE Symposium Series*, **86**, 47 (1990).

DISCLAIMER

This report was prepared as an account of work sponsored by an agency of the United States Government. Neither the United States Government nor any agency thereof, nor any of their employees, makes any warranty, express or implied, or assumes any legal liability or responsibility for the accuracy, completeness, or usefulness of any information, apparatus, product, or process disclosed, or represents that its use would not infringe privately owned rights. Reference herein to any specific commercial product, process, or service by trade name, trademark, manufacturer, or otherwise does not necessarily constitute or imply its endorsement, recommendation, or favoring by the United States Government or any agency thereof. The views and opinions of authors expressed herein do not necessarily state or reflect those of the United States Government or any agency thereof.

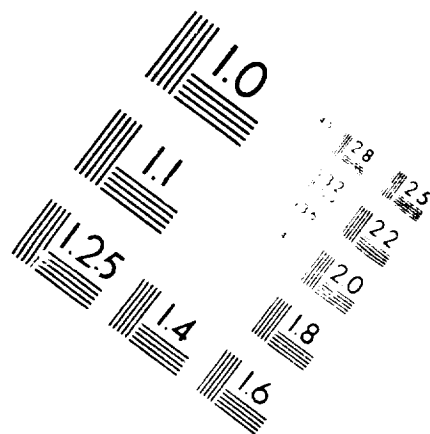
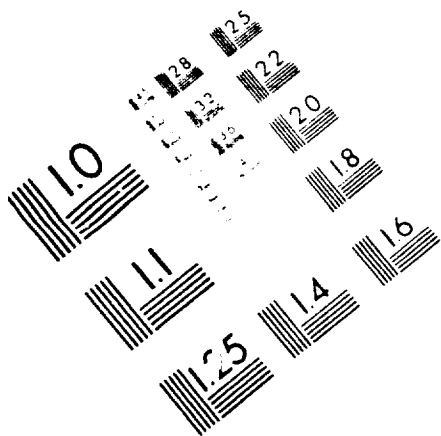


AIIM

Association for Information and Image Management

1100 Wayne Avenue, Suite 1100
Silver Spring, Maryland 20910

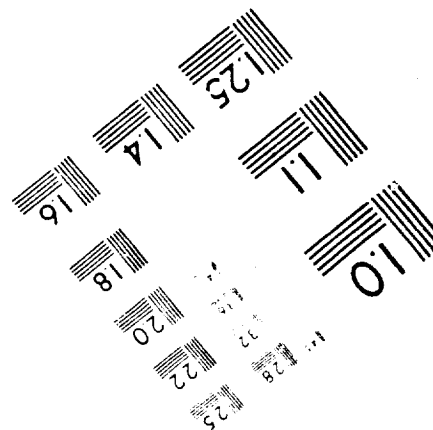
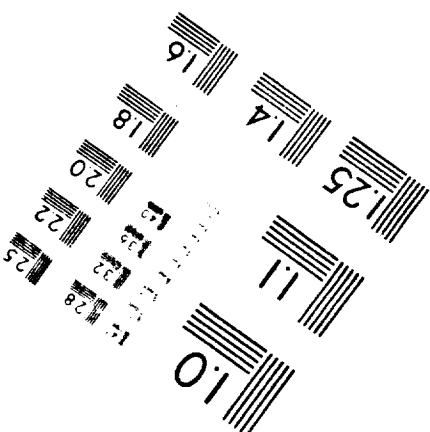
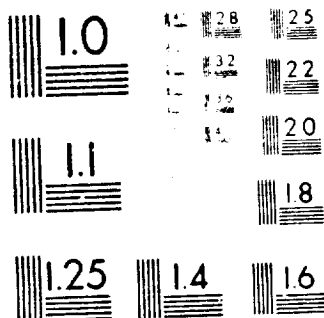
301-587-5212



Centimeter



Inches



MANUFACTURED TO AIIM STANDARDS
BY APPLIED IMAGE, INC.